Werk

Jahr: 1985
Kollektion: fid.geo
Signatur: 8 Z NAT 2148:58
Digitalisiert: Niedersächsische Staats- und Universitätsbibliothek Göttingen
Werk Id: PPN1015067948_0058
PURL: http://resolver.sub.uni-goettingen.de/purl?PPN1015067948_0058

LOG Id: LOG_0021
LOG Titel: Upper-mantle cross-section from California to Greenland
LOG Typ: article

Übergeordnetes Werk

Werk Id: PPN1015067948
PURL: http://resolver.sub.uni-goettingen.de/purl?PPN1015067948
OPAC: http://opac.sub.uni-goettingen.de/DB=1/PPN?PPN=1015067948

Contact

Niedersächsische Staats- und Universitätsbibliothek Göttingen
Georg-August-Universität Göttingen
Platz der Göttinger Sieben 1
37073 Göttingen
Germany
Email: gdz@sub.uni-goettingen.de

J Geophys (1985) 58:92–100

Journal of Geophysics

Upper-mantle cross-section from California to Greenland

D.V. Helmberger, G. Engen and S. Grand
Seismological Laboratory, California Institute of Technology, Pasadena, California 91125, USA

Abstract. Pure-path upper-mantle models appropriate for tectonic, shield and old ocean have been recently presented by Grand and Helmberger. This was accomplished by modeling a rather restricted data set of *S* and *SS* triplication waveforms as well as the beginning portion of the Love waves. A much larger data set of *S*, *SS* and *SSS*, etc. (multibounce *S*-wave triplications) with a mixture of tectonic paths is available. In particular, events usually occur at tectonic margins and are recorded on stable continents. We present results of modeling these observations for laterally varying structure, essentially along a profile from California to Greenland. The models are allowed to be locally dipping with the lithosphere thickening with age at the expense of a dwindling low-velocity zone. Lateral variation does not appear to be required for depths greater than 400 km along this particular profile. The best-fitting model has a large increase in lithospheric thickness near the Rocky Mountain Front, roughly an increase of 75 km in thickness over a horizontal distance of 400 km or less. The low-velocity zone, with a velocity of 4.4 km/s, is replaced by a much faster upper 300 km with velocities near 4.7 km/s or a 7% overall increase. The one-way travel time jumps by roughly 4 s across this boundary, which compares reasonably well with the direct *S* residuals obtained from deep earthquake data although the latter data show large scatter.

Key words: Upper mantle – *S* waves – Lateral variations – Synthetic seismograms

Introduction

In a recent paper (Grand and Helmberger 1984a), upper-mantle models appropriate for pure-path tectonic and shield regions were presented. By analyzing the (*SS*-*S*) travel times and waveform information, it became apparent that the seismograms could be partitioned into these two groups and interpreted in terms of vertical structure, see Fig. 1. Model SNA was derived from Canadian shield observations but has proven useful in modeling observations from other shields, Rial et al. (1984). The TNA model appears appropriate for younger oceanic structures and the more tectonic parts of western North America. Older oceans have a thicker lithosphere approaching the physical characteristics of the shield but conforming to the TNA model with depth as displayed in Fig. 1. Model ATL was derived for the 100-M-year-old portion of the western Atlantic, Grand and Helmberger (1984b).

In this paper, we will investigate the nature of the horizontal boundaries that connect the TNA and SNA provinces by modeling the seismograms that sample both areas.

The events used in this study occur along the western seaboard with recordings taken from the WWSSN and CSN stations. The locations of the stations and events are presented in Fig. 2. The events are also listed in Table 1. The reflection points at the free surface for the *SS* phases occur mostly in the midwest with the bottoming or turning points located in the western United States and in eastern Canada. The lateral structure across this region is probably three-dimensional, but the general trend is from tectonic to shield. Thus, to simplify a complex situation, we will assume that the data, associated with the station locations displayed in Fig. 2, can be averaged from north to south, i.e. observations at SHA of C2 can be compared to MDS of 05, etc.. In general, these seismograms do share common properties as pointed out earlier in Grand and Helmberger (1984a). Figure 3 displays representative seismograms from such paths and synthetics appropriate for the models TNA and SNA. Examining this figure, we see that the data are

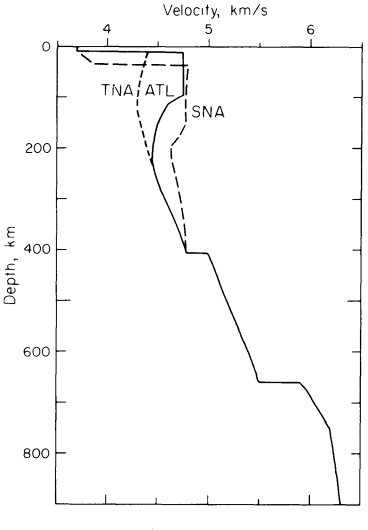

Fig. 1. Comparison of three pure-path models appropriate for tectonic (TNA), shield (SNA) and old oceanic (ATL)

Offprint requests to: V. Helmberger

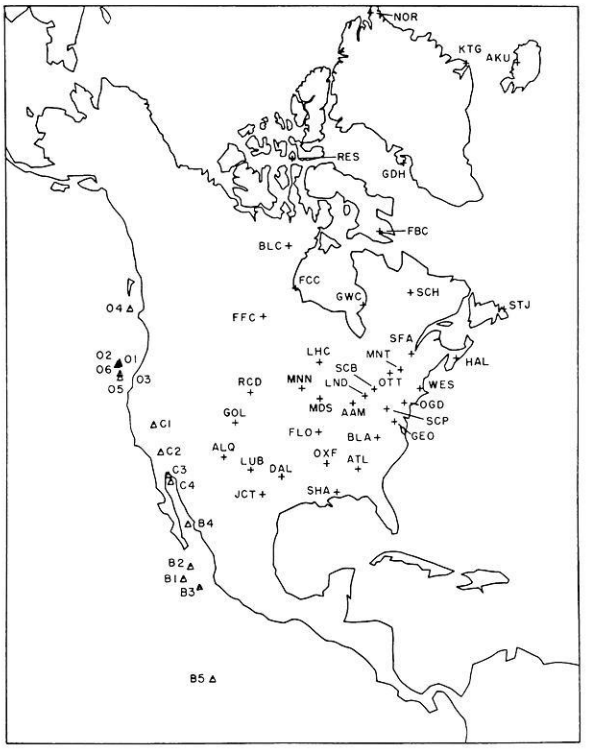

Fig. 2. Map of the North American continent locating stations and events. See Table 1 for a list of the events and identifications. Events are indicated by *triangles*, stations by *crosses*

closer to the SNA synthetics in timing but are more similar to the synthetics of TNA in waveform. The large amplitudes of *SS* at 37° in the TNA synthetics are caused by the constructive interference of arrivals from the 400-km transition and from the strong velocity gradient near the depth of 300 km, see Grand and Helmberger (1984a). A similar enhancement in the data of Fig. 3 occurs near 42° implying

Table 1. Event locations and identification

Event	Date	Location		Origin time		
01	1970 Nov. 26	43.8 N	127.5 W	03	11	43
02	1972 Oct. 25	43.4	127.7	01	01	41
03	1976 Jan. 27	43.6	127.4	16	06	48
04	1971 Mar. 13	50.6	130.0	23	31	36
05	1963 Aug. 22	42.0	126.4	09	27	03
06	1964 July 13	42.5	126.7	11	54	51
B1	1967 Jan. 23	19.9	109.3	20	25	38
B2	1966 May 23	21.3	108.7	11	51	27
B3	1966 Sept. 23	18.3	104.1	16	24	20
B4	1964 July 5	26.1	110.1	19	07	01
B5	1966 Sept. 23	10.3	104.1	16	24	20
C1	1978 Oct. 4	37.5	118.7	16	42	48
C2	1979 Mar. 15	34.3	116.4	21	07	17
C3	1966 Aug. 17	31.7	114.4	17	36	23
C4	1963 Nov. 19	30.9	113.8	08	23	12

a similar interpretation of arrival positions but with a 5° shift. This hypothesis is confirmed by this study where the overall objective will be to produce a laterally varying model from tectonic-to-shield explaining the *S*, *SS* and *SSS* data; essentially a cross-section from Baja, California to Greenland.

Parameterization and synthetics

In this section we will give a brief review of possible strategies in connecting TNA to SNA. One of the simplest means of accomplishing this objective is to allow the layers of constant velocity to change their thicknesses with position such that the lithosphere grows linearly with distance between TNA and SNA. A diagram showing this particular model variation is given in Fig. 4 along with representative ray paths used in generalized ray theory (GRT) on the left and WKBJ on the right. Note that a thin lithosphere has been added to the tectonic model and similarly a low-veloci-

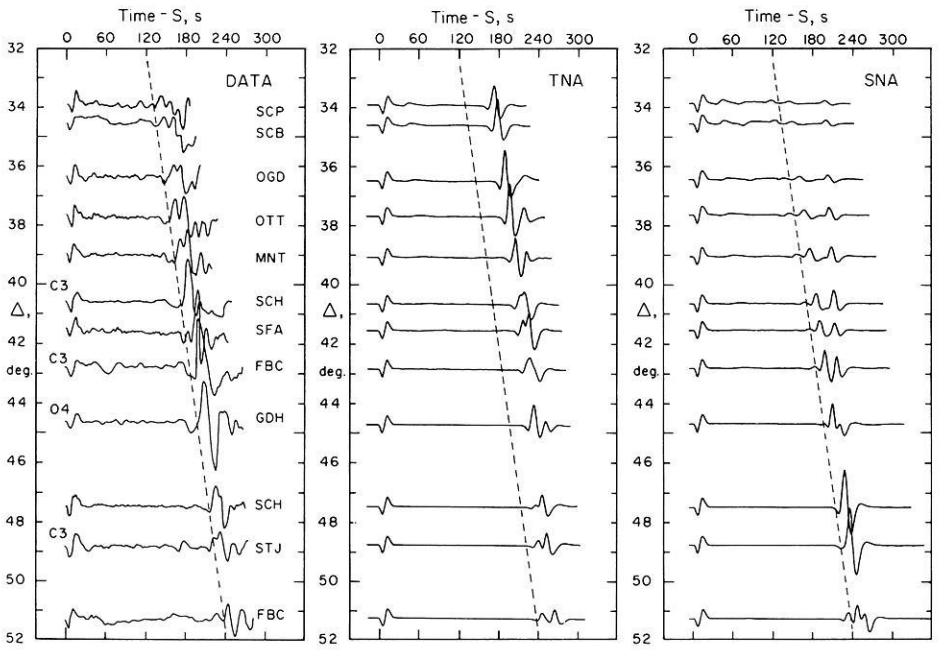

Fig. 3. Profiles of (*SS-S*) data along a mixed path compared with pure-path synthetics. The (*SS-S*) seismograms are from the event labeled B1 unless labeled otherwise, see Table 1

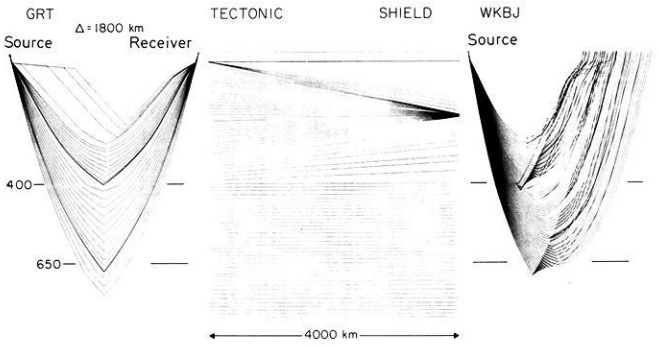

Fig. 4. Example of a simple linear transition from tectonic-to-shield along with ray paths appropriate for the two methods

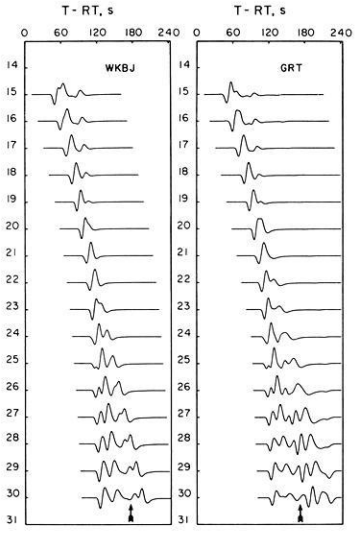

Fig. 5. Synthetics generated by the WKBJ and GRT methods for the linear model presented in Fig. 4

ty zone to the shield model. These zones are allowed to approach zero thickness and produce no effect on the synthetics for the pure paths.

Synthetics produced by GRT versus WKBJ are given in Fig. 5 where only the mantle arrivals are considered. The details of the generation of these synthetics are given in a companion paper, Helmberger et al. (1985), but the primary difference between the two methods can be seen in Fig. 4. GRT requires finding the ray paths that reflect off each layer boundary and connect the source to the receiver. This must be repeated for every station, a rather expensive procedure. In contrast, the WKBJ procedure uses only one set of rays that bracket the ranges of interest and the synthetics can be computed at any range. The general comparison of synthetic responses computed by the two methods agree about as well as in the flat-layered case, see Grand and Helmberger (1984a). The first arrival in the GRT result is relatively larger at the nearest distances due to tunnelling through the thin lid. At distances near 28°, the second negative peak in the WKB synthetics is too large compared to the GRT results. This arrival is the back branch of the 600-km triplication and such arrivals tend to be too large near the triplication tip, see Burdick and Orcutt (1978) for example. The last arrivals denoted by the arrows are truncation effects. Both can be eliminated or modified by adding more generalized rays, see Helmberger et al. (1985). However, we are primarily interested in mapping the position of the triplications and can tolerate some synthetic deficiencies. We will also omit the arrivals guided by the growing lithosphere, after giving a brief review of their properties.

A profile of synthetics containing the complete generalized ray set for the linear model is displayed in Fig. 6. As in a recent paper by Grand and Helmberger (1984a), we have broken up the rays into two groups; those that travel in the crust and lid or lithosphere, and those that return from below the low-velocity zone, LVZ. All the responses are normalized to the top trace. The short-period precursors to the long-period Love wave are multiples developing in the growing lid. Upper-mantle arrivals become contributors to the complete response at about 16.2° (1800 km) for this particular model. The two sharp spikes occurring in this trace are the onset of the 400 km triplication, essentially S and sS. Rays bottoming between 200 and 300 km produce the main arrivals. Synthetic seismograms assuming a $t^*_\beta = 3$ s and a far-field trapezoidal time history of (1,1,1) are given on the right. We probably over-attenuated the lid arrivals

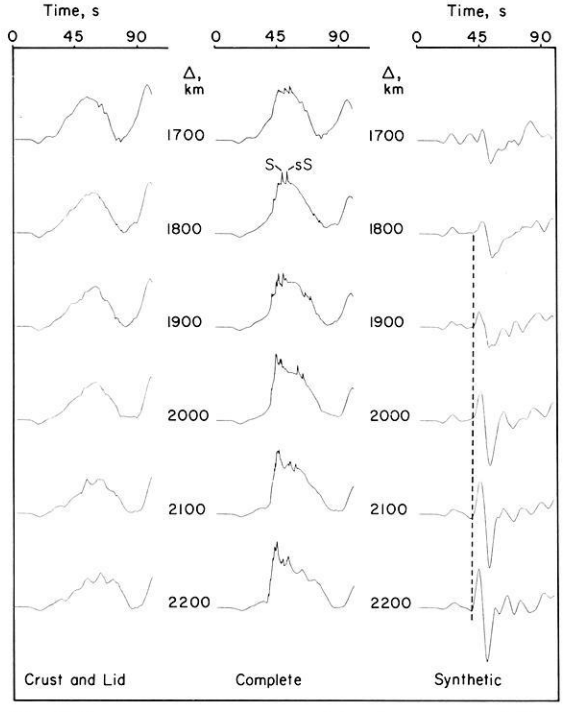

Fig. 6. Step responses generated by the crust and lid *on the left*, complete response *in the middle* and associated synthetics *on the right*. A trapezoidal time function with duration (1,1,1) was assumed for the time history and a $t^*_\beta = 3$ was chosen for a guess at the attenuation. The *dotted line* indicates the mantle arrival

in these synthetics since when we can see these precursors on long-period observations, they are also strong on the short-period records implying a high Q.

We do not see precursors for events near the western portion of the United States, see Grand and Helmberger (1984a), although they can be observed in Canada for some events located near the edge of the shield. Since we will be studying mostly western seaboard events, we will neglect lid arrivals and rely mostly on mantle arrivals in our model-

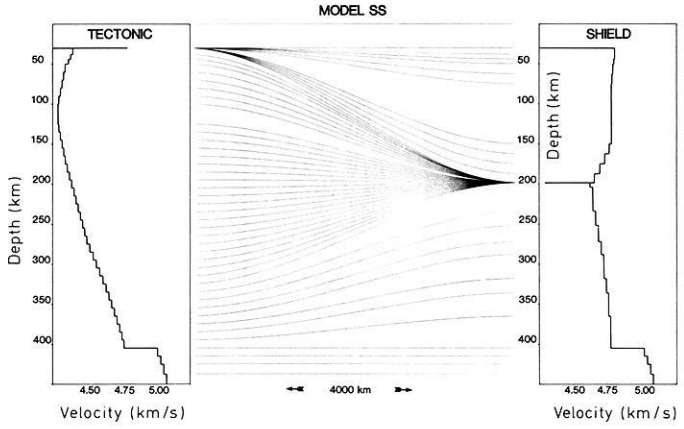

Fig. 7. Model SS connecting TNA to SNA with a slow transition above and below the 200-km LVZ

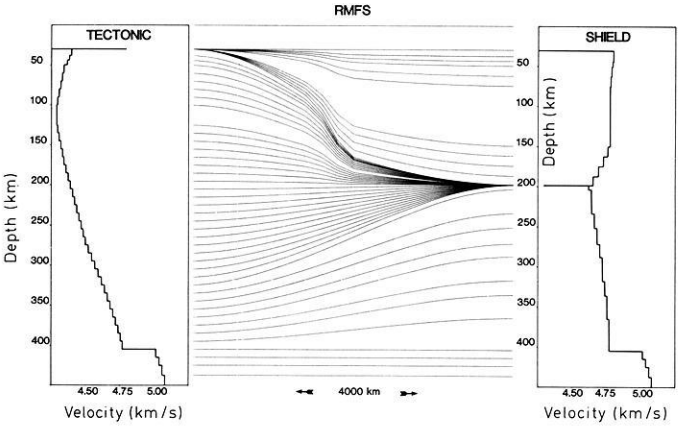

Fig. 9. Model RMFS connecting TNA to SNA with a fast transition above the LVZ occurring at about 1500 km from the western edge and a slow transition below the LVZ as in Fig. 7

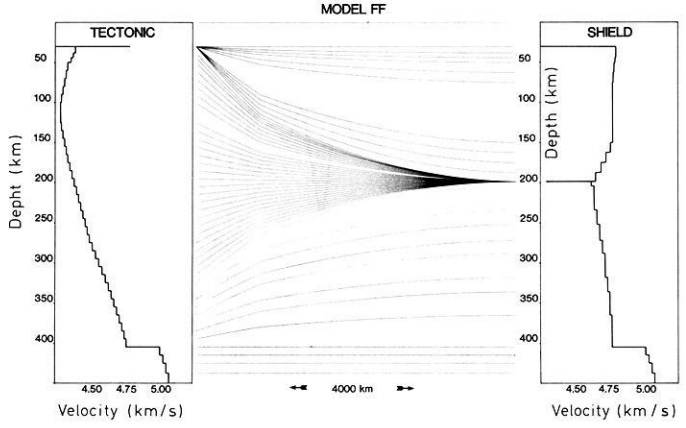

Fig. 8. Model FF connecting TNA to SNA with a rapid or fast transition above and below the LVZ

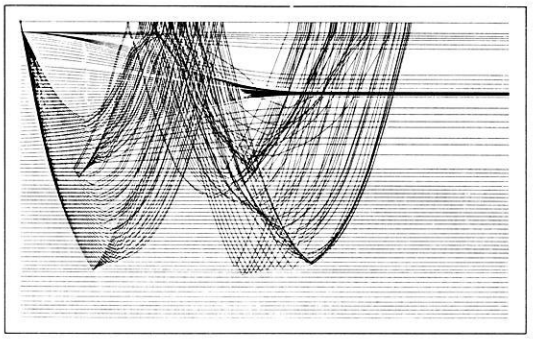

Fig. 10. Ray paths appropriate for SS as used in the WKBJ analysis

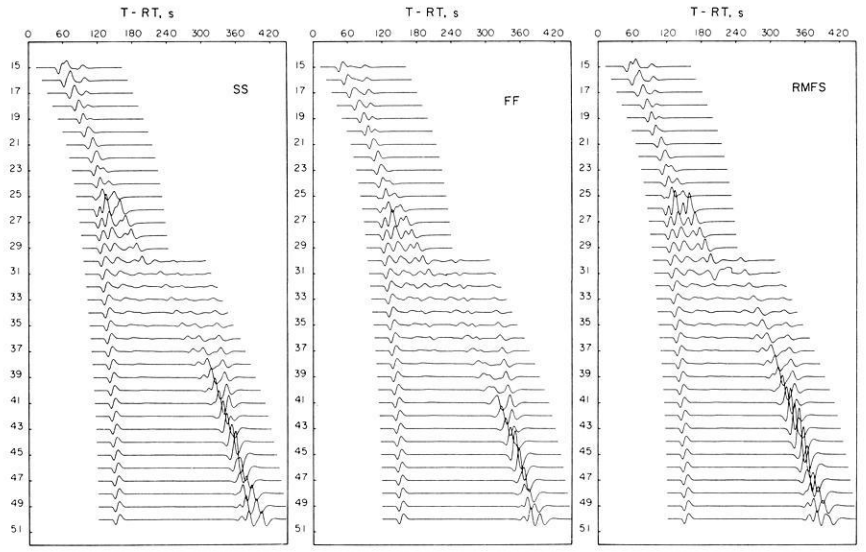

Fig. 11. Synthetic *S* and *SS* waveforms for the three possible models. The secondary arrivals traveling with relatively slow apparent velocities, located about 60 s after the first arrival at 30°, are inaccurate due to the WKBJ approximations as discussed in Fig. 5

ing efforts, essentially the phases *S*, *SS* and *SSS*. As mentioned earlier, we will be primarily interested in the shifts in triplications caused by the lateral variation.

Given our rather limited objectives, we choose to examine four basic types of model variation. Two of these models are given in Figs. 7 and 8. In the *SS* model, slow-slow, we allowed the model to start the change to shield slowly, from a depth of 40 km to the LVZ and from the LVZ to the 400-km discontinuity. In the FF model, fast-fast, the changes occur rapidly in both zones. The other two possibilities

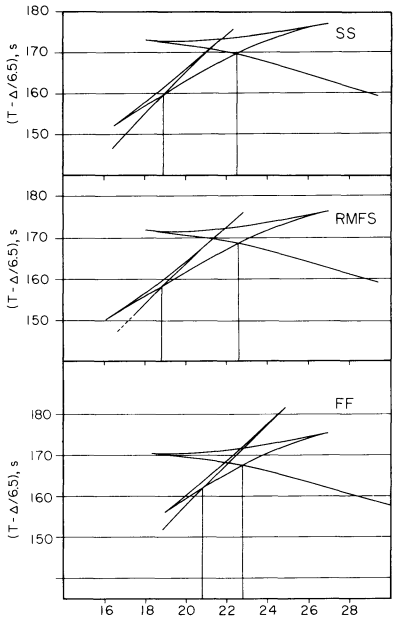

Fig. 12. Triplications appropriate for the three models

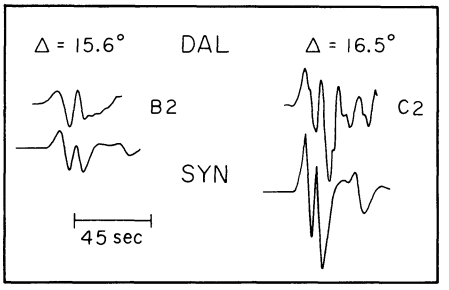

Fig. 13. Comparison of observations and synthetics at DAL, Texas. Synthetics have time history of (1,1,1)

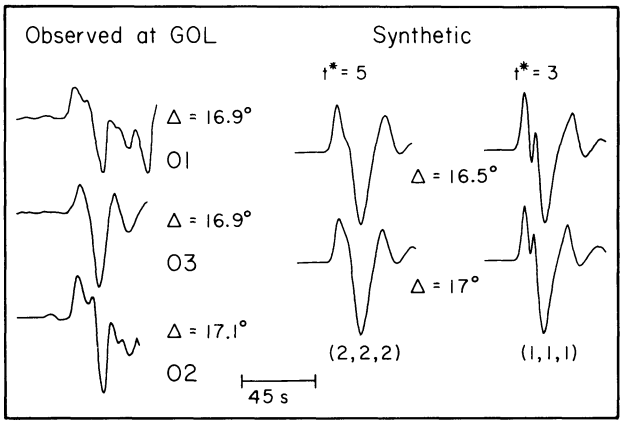

Fig. 14. Observations and synthetics at GOL, Colorado for various assumptions about time histories and attenuations. Note the longer-period first arrival in the data relative to the synthetics

were also considered; namely, models FS and SF. A modification of FS which we call RMFS is displayed in Fig. 9. The sharpness of the transition was also motivated by the rapid change in S travel-time residuals that apparently occurs near the Rocky Mountain Front, as discussed later.

The first stage in constructing the WKBJ synthetics is to compute the travel paths through the model for a family of ray parameters as displayed in Fig. 10. To insure accuracy, we must test for ray-path stability. This was done for the models displayed in Figs. 7, 8 and 9 by increasing the number of horizontal segments until the ray paths and resulting synthetics no longer changed. Triplication plots for these three models are displayed in Fig. 12. Synthetics containing the S and SS phases for these three models are displayed in Fig. 11 where the amplitutes are normalized to S. At the nearest distances, the 400-km triplication is especially apparent in the synthetics from the SS and RMFS models. All three models predict similar S synthetics beyond 21° as expected, given the uniformity in structure below 400 km. The SS phase appears similar as well, except that the ratio of the SS to S amplitude is different in the 35°–39° range. The strength of SS near 41° is distinctly different between the models, with the properties of the FF model least like the data. In the next section, we will compare the timing and waveforms of these synthetics with observations.

Comparison with observations

Selecting a set of observations to use for comparison with the synthetics discussed in the previous section may seem easy given the large numbers of events available. However, because of radiation pattern effects we may not obtain simple SH pulses along desired paths. SV coupled PL waves make working with rotated records difficult in many situations as pointed out earlier, Helmberger and Engen (1974). Thus, we chose only observations that are relatively naturally rotated or have stations located on SV nodes. The latter condition can be determined by studying the event teleseismically and, since we use only strike-slip events, the nodes for P and SV occur along the same azimuth. All the events used in this analysis are relatively shallow, less than 15 km. The standard depth used in all the synthetics was taken as 8 km, unless stated otherwise. A map displaying the stations and events used in the direct S waveshape analyses satisfying the above criterion is given in Fig. 2, as discussed earlier.

A comparison of some of these observations with the best-fitting model displaying the onset of the 400-km triplication is given in Figs. 13 and 14. Many of these events are quite small and have shorter time functions than the (1,1,1) assumed in Fig. 11, the event C2 with $M=5.2$ being a good example. The synthetics in these figures were computed with the WKBJ code and thus do not contain the tunnelled energy which appears as a long-period onset to the mantle S phase as displayed in Fig. 15. The effect disappears at larger ranges as the S phase leaves the shadow-zone boundary, in this case near 17°. We interpret the gradual beginning of the observed data at DAL and GOL as primarily due to this tunneled energy. These same events, as recorded at the more tectonic-type stations, TUC and ALQ, have sharp onsets with little evidence of any precursors. However, the thickness of the lithosphere is likely to be highly variable across the tectonic-shield transition and, given the uncertainty in attenuation effects and source durations, we do not think that detailed modeling of the precursor is justified at this stage. Nevertheless, the 400-km triplication is obvious in the data and this feature alone argues

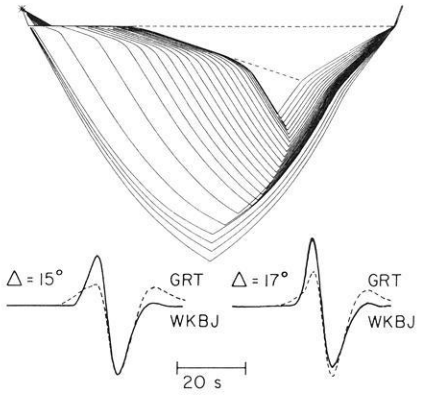

Fig. 15. GRT ray paths and synthetics appropriate for the various primary reflections making up the mantle *S* phase turning near the bottom of the LVZ. Also included are the WKBJ synthetics which do not contain the tunneled arrivals

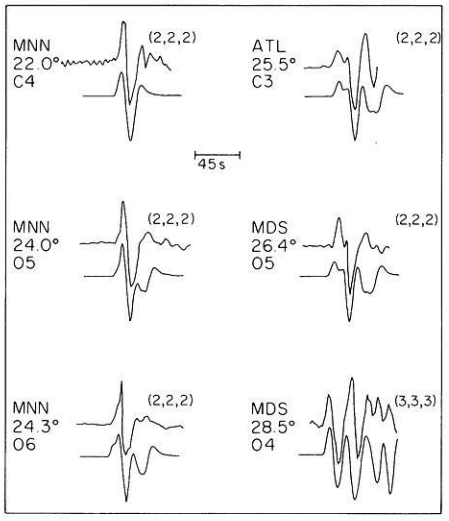

Fig. 16. Observations and synthetics displaying the interaction with the 600-km triplication. The various time histories are indicated for each synthetic

against a fast lateral transition below the LVZ such as that in model FF, seen in Fig. 8. Note that the 400-km triplication branch does not start until nearly 18° in the FF model, see Figs. 11 and 12.

A comparison of the RMFS synthetics with some of the observations displaying the strength of the 600-km triplication is given in Fig. 16. The comparison is quite good, indicating about the right separation between the triplication branches. But from Fig. 11 we note that the waveshapes are similar for all the models and model resolvability becomes difficult based on waveform data alone. Fortunately, the travel times of the direct *S* phase for the various models remain distinct and can be used as a constraint.

Travel-time considerations for the synthetic models and the observed first arrivals are given in Fig. 17. The travel times from the earlier study, Helmberger and Engen (1974), were included which, also, contain some of the larger and better located events in California. Since we have neglected the tunnelled arrivals in Figs 11 and 12, we should probably restrict our attention to distances beyond 17°. At these ranges and beyond, it appears that FF is slightly fast,

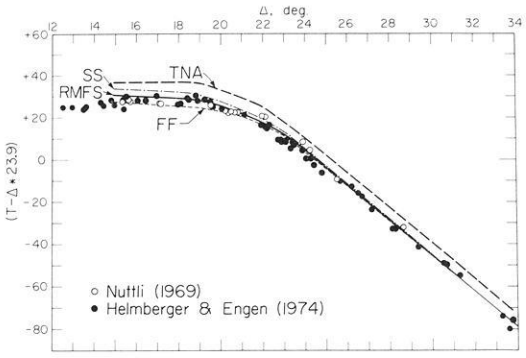

Fig. 17. Reduced travel times from observations, compared with WKBJ synthetics for possible models

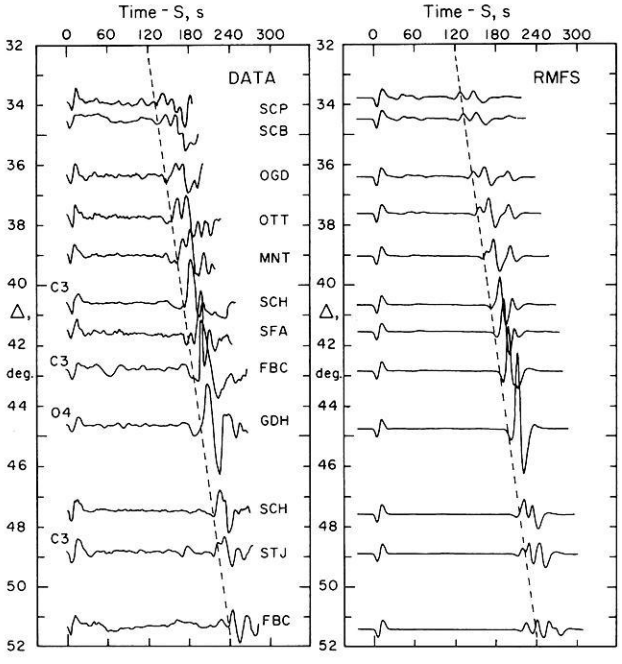

Fig. 18. Comparison of (*SS-S*) observations and synthetics. Unmarked seismograms are from event B1. Others have event numbers as in Table 1. Timing lines for *SS* are at the same time for both data and synthetics

whereas *SS* is too slow to 24°. The arrivals from the TNA model are late at all ranges. Comparison of the data with predictions from RMFS are quite good and, as we will show in the remainder of this section, the synthetics for this model fit the *SS* and *SSS* data as well.

Many of the travel times beyond 20° displayed in Fig. 17 are taken from the Borrego Mountain event, 1968. This event, as well as most of the larger events in the Imperial Valley, produce nearly identical *S*, *SS* and *SSS* seismograms along the profile to Greenland. Figure 18 displays a profile of west coast events from 34°–52° with appropriate synthetics for the RMFS model. The data profile and timing line is the same as displayed in Fig. 3.

In general, the RMFS model fits the data quite well. The double arrival in *SS* occurring in the data from 34°–39° is modeled well where the first arrival is coming from about a depth of 300 km and the second from the 400-km triplication. This pattern occurred at ranges 31–35° in the pure

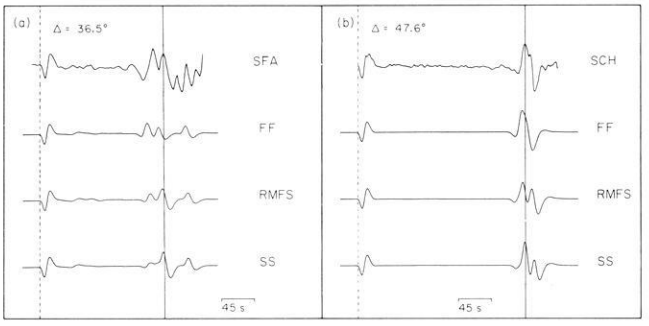

Fig. 19. Comparison of two example distances with corresponding synthetics

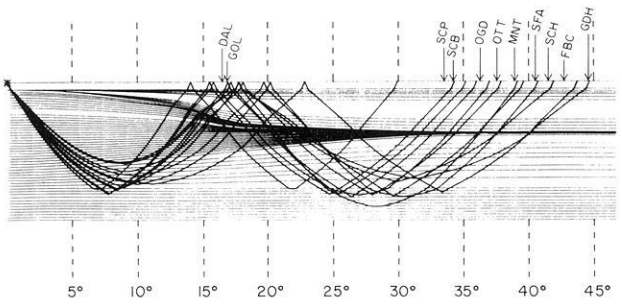

Fig. 20. Ray paths sampling the upper 400 km velocity structure as a function of lateral position

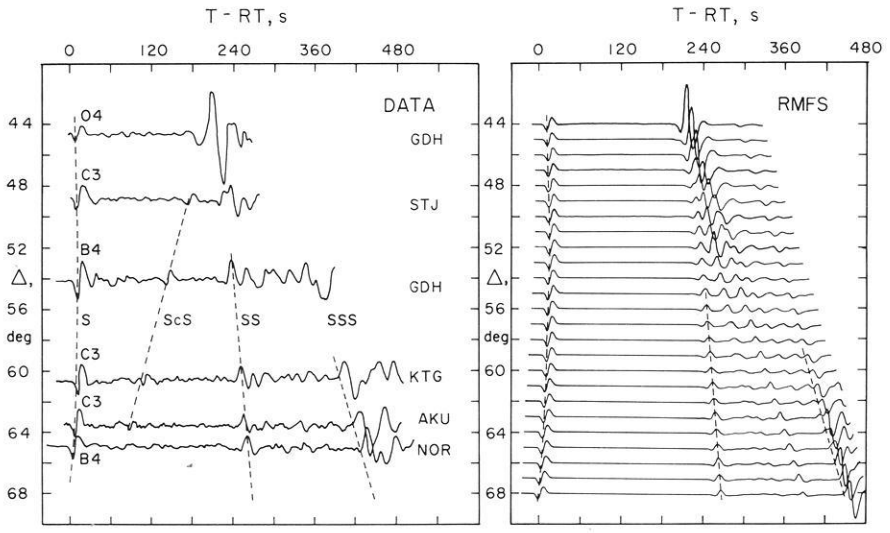

Fig. 21. Observations and synthetics. The *dotted lines* have been included for timing purposes

tectonic model. These two arrivals, in Fig. 18, merge at larger ranges, producing a strong peak. The 400-km and 600-km triplications cross near 45°. The ratio of *SS* to *S* becomes very large here, but depends critically on the source duration and the precise positions of the triplications.

It appears, from this profile, that the *SS* phase for our model is relatively fast out to about 38°. This would indicate that the lithosphere is possibly too thick at epicentral distances less than 15° and should grow more slowly before then, with perhaps a sharper jump at the Rocky Mountain Front. Other profiles of data along this azimuth are displayed in Grand and Helmberger (1984a). Some of these events are located far enough to the south to shift the interference pattern with respect to the stations.

There is a tendency for the ratio of *S* to *SS* amplitudes to vary somewhat from event to event. This feature of the data has not been addressed here but probably is related to small amounts of dip-slip components present in these events. Corrections for such effects would be required if the ratios were being used for attentuation measurements.

The other two models produce reasonable fits to this profile, although the synthetics for *SS* are too slow. A comparison of two key distances is given in Fig. 19 where, as in the direct *S* case, the FF model appears slightly too early, particularly at $\Delta = 36.5°$. At $\Delta = 47.6°$, the FF synthetic fits the observed waveform quite well. Note that the SFA observation is from event C3 at the California-Baja border, while the observation at SCH is of the B1 event near the tip of Baja. The first leg of *SS* samples a zone near GOL for the former path and near JCT for the latter path. See Fig. 2. From many detailed comparisons between the various observations and proposed models, we reach the conclusion that substantial three-dimensional structure is present in the data. However, the RMFS model appears to be a good, average two-dimensional model.

A cross-section of velocity structure with the *SS* ray paths appropriate for those arrivals bottoming near the 400-km discontinuity is given in Fig. 20. Note that the ray segments become asymmetric when each leg samples different structure. The figure gives an indication of station location along the model. However, keeping in mind that the model is truly three-dimensional and this is a two-dimensional slice, it is probably true that the structures at DAL and GOL for example are not alike, although the distances from the sources are approximately the same. Therefore, this figure is meant only as a guide to the parts of the models which affect the timing and waveshapes of the seismograms at different stations. It does indicate that for *S* arrivals along the Rocky Mountain Front, RMF, mostly tectonic structure is sampled, but the shape of the RMF and the actual location of the station along it will vary

from north to south. Also, one can see that for distances beyond about 30° the second segment of *SS* travels almost exclusively in the shield.

An extension of the data profile to larger distances and including *SSS* is displayed in Fig. 21 along with synthetic predictions for model RMFS. These data are somewhat contaminated by *SV* since *SH* is no longer in the center of the radiation loop. This may be the reason for the distortions in *SS* at some of the stations such as KTG. The dotted lines have been added at the same positions on both sections, indicating an excellent fit to the relative travel times. Note that *SSS* peaks near 66° in both the data and synthetics. This feature is again caused by the crossing of two triplications. The phase *SSSS* is apparent in European stations for these same events with peak amplitude ratios occurring at STU (88°). No attempt was made at modeling these data because of the mixture of paths encountered in crossing the extreme tip of the North Atlantic. An abundance of direct *S* and *SS* data are available for modeling this region and will be discussed in a later paper.

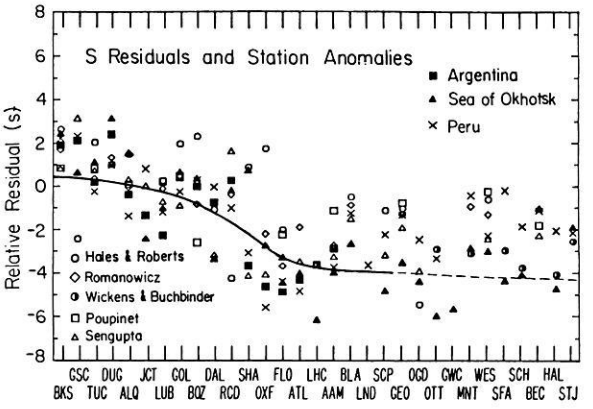

Fig. 22. Comparison of relative JB residuals with synthetics (RMFS), modified from Lay (1983). The line is dotted beyond SCP since many of these stations are near the Atlantic coast and are expected to be late, see Grand and Helmberger (1984b)

Discussion

The RMFS model fits a relatively large amount of travel-time and waveform data and implies a rapid horizontal gradient in velocity near the Rocky Mountain Front. Exactly where the model has this sharp change relative to the surface geology is uncertain because of the averaging process discussed earlier. Nevertheless, it is interesting to compare the predicted delay time produced by this model with the observed travel-time residuals, see Fig. 22. We suppose that stations BKS and GSC are near the western edge of the model and plot the relative travel-time delay appropriate for vertical incidence. Correcting the data to vertical incidence would reduce the total variation by about 15% so that the overall agreement between the model and data is quite good. Note that the most rapid changes in the data occur near stations RCD and DAL with about a 4-s shift in travel times. These stations show considerable scatter with strong evidence of azimuthal dependence. Some of this scatter is probably caused by slab extension in the source region, Jordan (1977), and anomalies in the lower mantle, Lay (1983). However, the analysis presented here would not eliminate the possibility of horizontal gradients sharper than those suggested by RMFS, and if such strong transitional boundaries exist we might expect to see some particularly interesting travel-time patterns along the boundary. Note that such geologic boundaries would probably not be linear as supposed in this study. A manifestation of such structure on the character and waveshapes of recorded teleseismic signals has not been noted in the literature but, on the other hand, the data and methods required to synthesize such effects are only now becoming available.

There is a tendency for the *S* residuals for stations near the eastern seaboard to become less negative. For instance, the values observed at Bermuda, BEC, appear to be only slightly smaller than predicted by JB, a result completely compatible with the ATL model presented in Fig. 1, see Grand and Helmberger (1984b).

Adding a section of old-ocean-type structure to the laterally varying model does not generate any improvement in the synthetic matching for the Greenland stations, see Fig. 23. Apparently, the slow-down in the third bounce of the *SSS* path caused by such a modification is not supported by the data. In this case, the third bounce-point is near the Baffin Islands which is apparently underlain by shield structure. This result is again compatible with the earlier study by Grand and Helmberger (1984a).

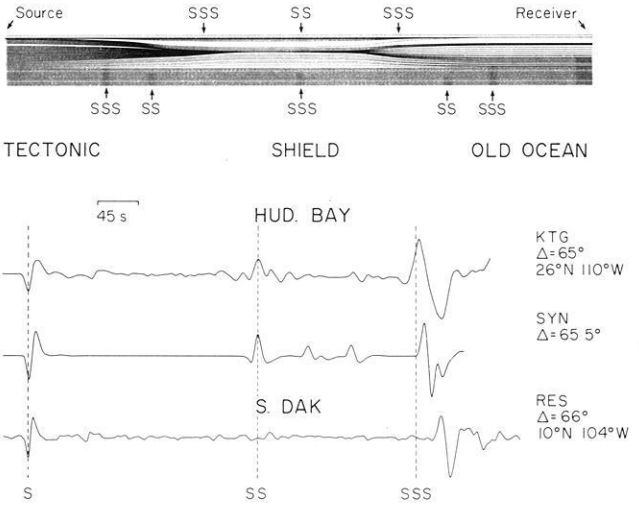

Fig. 23. Possible velocity cross-section, upper 400 km, from California to Greenland *on the top* with corresponding synthetic *on the bottom*. The source locations for the two observations are given below the station names, see B4 and B5 in Fig. 2. The surface bounce-points for the *SS* phases are near Husdon's Bay and South Dakota, respectively

The observation at RES was included in Fig. 23 to convey some of the rapid variation observed at other azimuths. The *SSS* phase is strong, but more than 20 s late relative to the paths to Greenland. The *SS* phase is weak, with its bounce-point occurring in South Dakota. Other observations along this path show clearer *SS* signals which are more normal in strength but several seconds late. These features appear to be another manifestation of the strong horizontal gradient associated with the stable continent transition which is undoubtedly complex in nature. Hopefully, by examining the many paths that cross the region we will be able to construct a truly three-dimentsional model and, perhaps, the multi-bounce *S* phases will prove to

be a useful tool in conducting "structural seismology" studies as defined by Jordan (1979).

In summary, we have used the multi-bounce *SH* phases to study the nature of the horizontal transition between the tectonic province in the western United States and the more shield-like continental platform. We relied on the travel times of direct *S* over the range 15°–30° and the synthetic modeling of *S* from 15°–27°, *SS-S* from 36°–52° and *SSS-SS-S* from 44°–66°. Homogeneous layering was assumed in the modeling, but we allowed the layers to change their thickness with position. The preferred model has a smooth transition from west to east at depths greater than 200 km, but a rather abrupt change in lithospheric thickness occurring near the Rocky Mountain Front. The vertical one-way travel-time anomalies computed for this model are in reasonable agreement with measured teleseismic travel-time residuals. A jump of about 4 s is associated with crossing the Front. The method is relatively easy to use and can be employed in investigations of remote regions where little direct data is available.

Acknowledgements. We would like to thank Cindy Arvesen for helping with the data processing and drafting. This work was supported by the National Science Foundation Grant EAR-8306411 and by the Air Force Office of Scientific Research Grant F49620-83-C-0025. Contribution 4173, Division of Geological and Planetary Sciences, California Institute of Technology, Pasadena, California 91125.

References

Burdick, L.J., Orcutt, J.A.: A comparison of the generalized ray and reflectivity methods of waveform synthesis. Geophys. J. R. Astron. Soc. **58**, 261–278, 1978

Grand, S.P., Helmberger, D.V.: Upper mantle shear structure of North America. Geophys. J.R. Astron. Soc. **76**, 399–438, 1984a

Grand, S.P., Helmberger, D.V.: Upper mantle shear structure beneath the Northwest Atlantic Ocean. J. Geophys. Res. **89**, 11465–11475, 1984b

Hales, A.L. Roberts, J.L.: The travel times of S and SKS. Bull. Seismol. Soc. Am. **60**, 461–489, 1970

Helmberger, D.V., Engen, G.R.: Upper mantle shear structure. J. Geophys. Res. **79**, 4017–4028, 1974

Helmberger, D.V., Engen, G.R., Grand, S.: Notes on wave propagation in laterally varying structure. J. Geophys. **58**, 82–91, 1985

Jordan, T.H.: Lithospheric slab penetration into the lower mantle beneath the Sea of Okhotsk, Geophys. J.R. Astron. Soc. **43**, 473–496, 1977

Jordan, T.H.: Structural geology of the earth's interior. Proc. Nat. Acad. Sci., USA **76**, 4192–4200, 1979

Lay, T.: Localized velocity anomalies in the lower mantle. Geophys. J.R. Astron. Soc. **72**, 483–516, 1983

Nuttli, O.W.: Travel times and amplitudes of S′ waves from nuclear explosions in Nevada. Bull. Seismol. Soc. Am. **59**, 385–398, 1969

Poupinet, G.: Hétérogénéités du manteau terrestre déduites de la propagation des ondes de volume: implication géodynamique. Thèse présentée à l' Université Scientifique et Médicale de Grenoble, 1977

Rial, J.A., Grand, S., Helmberger, D.V.: A note on lateral variation in upper mantle shear-wave velocity across the Alpine front. Geophys. J.R. Astron. Soc. **77**, 639–654, 1984

Romanowicz, B.A., Cara, M.: Reconsideration of the relations between S and P station anomalies in North America. Geophys. Res. Letts. **7**, 417–420, 1980

Sengupta, M.K.: The structure of the earth's mantle from body wave observations. M.S. Thesis, Massachusetts Institute of Technology, 578 pp, 1975

Wickens, A.J., Buchbinder, G.G.R.: S-wave residuals in Canada, Bull. Seismol. Soc. Am. **70**, 809–822, 1980

Received February 20, 1985; revised version June 18, 1985
Accepted June 25, 1985